

AUS Repository

Mathematical modeling of microbubble cavitation at 70 kHz and the importance of the subharmonic in drug delivery from micelles

Item Type	Peer-Reviewed;Article;Postprint
Authors	Diaz de la Rosa, Mario A.;Husseini, Ghaleb;Pitt, William G.
Citation	Mario A. Díaz de la Rosa, Ghaleb A. Husseini, William G. Pitt, Mathematical modeling of microbubble cavitation at 70kHz and the importance of the subharmonic in drug delivery from micelles, Ultrasonics, Volume 53, Issue 1, 2013, Pages 97-110, ISSN 0041-624X, https://doi.org/10.1016/j.ultras.2012.04.004 .
DOI	10.1016/j.ultras.2012.04.004
Publisher	Elsevier
Download date	2026-03-07 06:33:15
Link to Item	http://hdl.handle.net/11073/21298

Mathematical modeling of microbubble cavitation at 70 kHz and the importance of the subharmonic in drug delivery from micelles

Mario A. Díaz de la Rosa ^a, Ghaleb A. Hussein ^{b,†}, William G. Pitt ^a

^a Department of Chemical Engineering, Brigham Young University, Provo, UT 84602, United States ^b Chemical Engineering Department, American University of Sharjah, Sharjah, United Arab Emirates
<https://doi.org/10.1016/j.ultras.2012.04.004>

article

info

Abstract

Article history:

Received 11 October 2010

Received in revised form 4 April 2012

Accepted 15 April 2012

Available online 23 April 2012

Keywords:

Bubble dynamic behavior

Cavitation

Ultrasound

Subharmonic

Doxorubicin drug delivery

In order to gain insight into the experimental observation of ultrasound-induced release of drugs from micelles, we modeled the dynamic oscillations of a 10- μm -diameter bubble insonated at 70 kHz. The Parlitz modification of the Keller–Miksis model was employed to generate bubble dynamics over a wide range of mechanical index values. The resulting Poincaré maps and bifurcation diagram show that bubble oscillations bifurcate at a MI value of 0.32, then return apparently to a single mode before displaying a sudden onset of chaotic behavior at 0.35. The experimental release of drug from micelles occurs at a MI value of 0.37 and correlates with the intensity of the subharmonic in ($\text{I W}/\text{cm}^2$) of the acoustic spectrum. The dynamic model shows the return to single mode at a MI value of 0.43, and bifurcation leading to chaos at values above 0.5. The correlation between the chaotic behavior predicted by the model and drug release hints at insonation conditions that could facilitate drug delivery.

2012 Elsevier B.V. All rights reserved.

1. Introduction

The study of polymeric micelles as drug delivery vehicles has revealed a number of advantages over other vehicles, including (1) structural stability, or slow dissolution levels below their critical micelle concentration; (2) prolonged shelf life; (3) long circulation time in blood and stability in biological fluids; (4) an appropriately large size to prevent renal excretion and yet (5) small enough to allow extravasation at the tumor site; (6) simplicity in drug incorporation (no need for covalent bonding to the carrier); and (7) drug delivery independent of drug character. Our investigation into the nature of ultrasonically activated drug release from polymeric micelles [1–8] revealed that there is an acoustic pressure threshold required to initiate drug release, and that beyond this threshold the amount of drug release correlates with the intensity of the subharmonic of the applied ultrasonic frequency [9,10]. We have performed extensive experimental research to find the parameters that maximize ultrasonic-induced drug release including frequency (20 kHz to 1.5 MHz), power density (for example at 70 kHz the power density was varied between 0.1 W/cm^2 and 0.8 W/cm^2), temperature (25 C, 37 C and 56 C), and micelle crosslinking. Among our experiments, the most release was observed at 70 kHz and 0.8 W/cm^2 . The correlation of drug release with the subharmonic amplitude was previously unknown until we performed these more detailed acoustic experiments at 70 kHz in which acoustic collection was combined with fluorescence detection of the drug release. The correlation with the subharmonic implicated the role of bubble cavitation, as others had also correlated stable and inertial cavitation with the subharmonic signal [11–22]. These results raise questions about the nature of the bubble oscillations that generate the subharmonic

signal (and correlate with drug release) at 70 kHz and their potential interaction with drug-carrying micelles. We address these questions in this paper using the tools of bubble dynamics. Hopefully this study will shed light on the optimum insonation to apply to micelles for controlled drug delivery using ultrasound.

All theoretical investigations of the dynamics of bubble oscillations begin with the classic Rayleigh–Plesset equations (essentially a form of the momentum conservation equations) and its numerous modifications, which are reviewed in detail in [15]. The basic equations assume a spherical, isolated, internally homogeneous bubble in an infinite liquid medium in the absence of thermal and mass transfer effects. Modifications to that formulation address these limitations and include the assumption of polytropic gas behavior, the addition of liquid compressibility effects, and the inclusion of heat and mass transfer effects [15,23–28]. Further work addresses the behavior of bubble clouds or clusters [29–31] and sonoluminescence [32,33].

Treatments that approach the bubble equations from a dynamical systems perspective [23,34–40] are relevant to our drug delivery system, as they are among those that have reproduced subharmonic emission thresholds [19,23,30,33–36,40–44]. In particular, Lauterborn used the qualitative tools of chaos physics (dynamical systems) [23] to interpret the behavior of bubble oscillations [24], revealing a glimpse of the rich, complex dynamics inherent within the governing equations. In this paper, we similarly analyze bubble oscillations at 70 kHz. Specifically, we seek to find the same (or analogous) experimental acoustic signatures through modeling and to explore bubble behavior in a neighborhood of the drug release thresholds found previously [9,10]. Our overall goal is to answer two significant questions: (1) what type of

bubble behavior is responsible for drug release in our in vitro system and (2) precisely under what conditions can drug release be engineered?

2. Methods and materials

2.1. Drug encapsulation in Pluronic micelles

Doxorubicin (Dox) was obtained from the University of Utah Hospital (Salt Lake City, UT) in a 1:5 mixture with lactose; it was dissolved in phosphate buffered saline (PBS) and sterilized by filtration through a 0.2 μm filter.

Stock solutions of Pluronic P105 (BASF, Mount Olive, NJ) were prepared by dissolving P105 in a PBS solution to a final concentration of 10 wt%. Dox was dissolved into the P105 solutions at room temperature to produce a final Dox concentration of 10 mg/ml in 10 wt% Pluronic. The same drug concentration was also prepared in PBS.

2.2. Measuring ultrasound-triggered release of Dox from Pluronic P105 micelles

The experimental system employed in this research was presented previously [9,10]. The 488 nm beam of an argon ion laser (Ion Laser Technology, Model 5500 A) was directed through a beam splitter attenuator (metal film neutral density attenuator). The intensity of the split portion of the beam was measured by a photo detector (Newport Model 818-SL with 835 display) and was used to monitor the laser power throughout our experiments. In the newly modified apparatus, the other portion of the beam was directed into one branch of a dual branch fiber optic bundle (# DF13036M, Edmunds Optics, Barrington, NJ) that directed the light into an acoustically transparent plastic (cellulose butyrate) (Tulox Plastics, Marion, Indiana) tube, with a diameter of 2.54 cm, filled with the Dox solution. The laser light exited the fiber optic bundle in a cone of light. Any Dox within the cone of light absorbs at 488 nm and emits fluorescent light centered at 580 nm in all directions. In the same fiber optic bundle are fibers that collect and direct the fluorescence to a detector. The geometry of the fiber optic is such that 99% of the collected fluorescence originated from within 3 mm of the fiber optic tip. The fluorescence signal was directed through the second branch of the fiber optic bundle through a multimode dielectric band and filter (Omega Optical Model 535DF35) to a silicon detector (EGSG Model 450-1). The filter was used to cut off any emissions with a wavelength below 500 nm, including any Rayleigh-scattered laser light. The photo detector signal was sent to an oscilloscope (Tektronix Model TDS 3012) from which it was captured and subsequently stored on a computer for further processing. This apparatus can measure the amount of acoustically-activated Dox release from micelles because Dox exhibits a decrease in fluorescence in contact with an aqueous solution.

This is precisely the case when Dox is released from Pluronic micelles, and it follows that the magnitude of decrease in fluorescence intensity upon application of ultrasound provides a quantifiable measure of drug release.

The decrease in fluorescence of the encapsulated drug solution was assumed to be directly proportional to the amount of drug released relative to a known baseline. The fluorescence of Dox in PBS, in the absence of Pluronic, was measured to simulate 100% release. Then the percent release was calculated using the following equation:

$$\%Release = \frac{I_{P105} - I_{US}}{I_{P105} - I_{PBS}}$$

where I_{US} is the fluorescence intensity upon exposure to ultrasound, I_{PBS} is the fluorescence intensity in a solution of free Dox in PBS, and I_{P105} is the intensity recorded when the drug was encapsulated in Pluronic P105 (which corresponds to 0% release or 100% encapsulation).

In these experiments, the fluorescence intensity of the drug in PBS was measured both with and without application of ultrasound. Ultrasound was applied using a 70-kHz ultrasonication bath (SC-40, Sonicator, Copiaque, NY) equipped with a single piezoceramic transducer that is driven at about 70 kHz. The sonicating bath chamber was 12.7 cm \times 12.7 cm and filled with water to a height of approximately 11 cm. Attached at the center of the underside of the bath was a piezoelectric transducer of 7.5 cm diameter. The best description of the waveform is that of a 70-kHz wave that is amplitude modulated sinusoidally at about 0.12 kHz. The bath was powered by 60 Hz AC voltage coming from a variable AC transformer (variac). The voltage from the variac to the sonicating bath was varied to produce differing intensities of ultrasound. To execute the experiments, the end of the fiber optic was positioned at an acoustically intense position in the ultrasonication bath. The bath was filled with degassed water and the tube surrounding the fiber optic was filled with the solution of Dox in PBS. Fluorescence emissions were collected for different voltages applied to the ultrasonication bath. Then, without changes in the experimental set-up, the Dox solution in PBS was carefully removed and replaced with a Dox solution of the same concentration in Pluronic micelles. During insonation, fluorescence dropped due to Dox coming in contact with the surrounding aqueous environment. Several fluorescence measurements were made at each intensity setting and averaged ($n = 8$ when $I > 0.27 \text{ W/cm}^2$ and $n = 4$ when $I < 0.27 \text{ W/cm}^2$).

2.3. Acoustic measurements

Ultrasonic power density measurements were obtained using a calibrated hydrophone (Bruel and Kjaer model 8103, Decatur, GA) whose response was measured with an oscilloscope. After measurements of Dox fluorescence, the fiber optic was replaced with the hydrophone in the same location, and the hydrophone

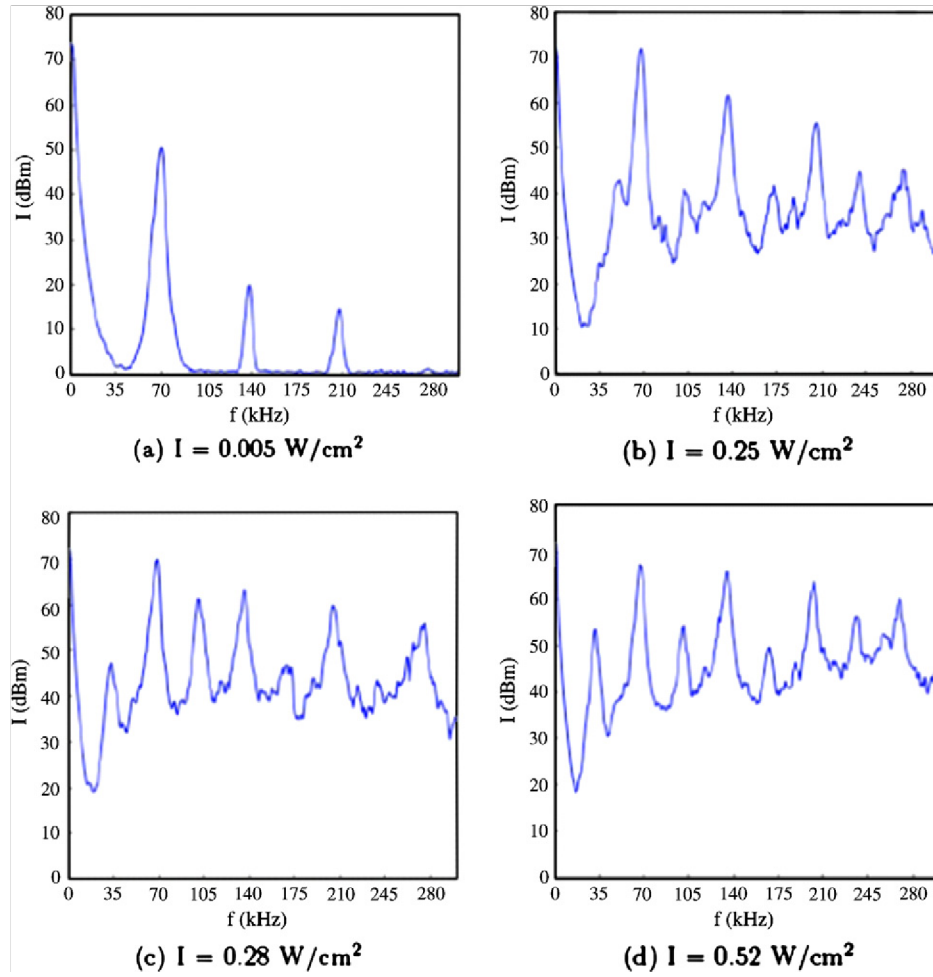


Fig. 1. Acoustic spectra for 70 kHz insonation at (a) power density (I) = 0.005 W/cm², MI = 0.05; (b) I = 0.25 W/cm², MI = 0.33; (c) I = 0.28 W/cm², MI = 0.35; and (d) I = 0.52 W/cm², MI = 0.47.

response was recorded at the same settings as used for the fluorescence measurements. The average acoustic intensity was calculated from $I \frac{1}{4} V_{\text{rms}}^2 Q^2 = Z$ where Q is the calibration factor, Z is the acoustic impedance ($1.5 \cdot 10^6$ kg/m² s), and V_{rms} is the rootmean-squared voltage of the hydrophone signal.

Acoustic spectroscopy was used to monitor the vibrations of the cavitating bubbles in the ultrasonic field at the power settings used in the release measurements. The hydrophone signal was directed to a spectrum analyzer (Agilent E4401B), from which the acoustic spectrum was obtained. Because the hydrophone had about the same diameter (9.5 mm) as the fiber optic bundle (9 mm), any measured perturbation in the acoustic field caused by the presence of the hydrophone would be similar to those caused by the fiber optic bundle.

We selected 70-kHz insonation in this study for several reasons. Not only are 70-kHz transducers available in our lab, but this frequency has been used successfully for drug delivery to cells and animals [5,8]. Furthermore, this frequency has been studied by Parlitz [35], and we could check our numerical results against his to validate our equations and execution of the numerical model.

2.4. Mathematical model of bubble oscillator

In this research, we used several models of spherical bubble oscillation dynamics with various levels of complexity, which we present below. The Noltingk–Neppiras–Poritsky modification of the classic Rayleigh–Plesset equation is given as [15]:

$$\frac{p_g(T_\infty) - p_\infty(t)}{\rho_L} + \frac{p_{G_0}}{\rho_L} \left(\frac{R_0}{R}\right)^{3k} = R\ddot{R} + \frac{3}{2}\dot{R}^2 + \frac{4v_L\dot{R}}{R} + \frac{2S}{\rho_L R} \quad (2)$$

All terms are defined in Table 1. This modification to the original Rayleigh–Plesset formulation accounts for the bubble contents as a polytropic gas. We are interested in a bubble driven by a sinusoidal driving pressure

$$p_\infty(t) = p_{\text{stat}} + A \sin(2\pi ft). \quad (3)$$

We solved the following system of differential equations by means of MATLAB's adaptive ODE solver ode45:

$$\begin{aligned} \dot{R} &= u \\ \dot{u} &= \frac{p_v(T_\infty) - p_{stat} - A \sin(2\pi\Theta)}{\rho_L R} + \left(\frac{p_{G_0}}{\rho_L R}\right) \left(\frac{R_0}{R}\right)^{3k} - \frac{3}{2} \frac{u^2}{R} \\ &\quad - 4\nu_L \frac{u}{R^2} - \frac{2S}{\rho_L R^2} \\ \dot{\Theta} &= f \end{aligned} \quad (4)$$

where the velocity of the gas–liquid interface is $u = \dot{R}$ and $\Theta = f t \text{ mod } 1$.

Unfortunately, this formulation is incapable of yielding reliable information around the moment of collapse (when high temperatures and pressures are generated) since it fails to account for liquid compressibility [15]. Keller and Kolodner [45] and later Keller and Miksis [46] rectified this problem by introducing the

Keller and Miksis equation are equivalent up to terms of order (c^{-2}) , which terms are ignored during the derivation of Parlitz. Accordingly, we used the Parlitz modification of the Keller–Miksis model for the results presented in this paper. The modification comes in the pressure driving term. This modification preserves the equation as an autonomous system that is solvable while also keeping the nonlinear representation of our system. The equation is

$$\left(1 - \frac{\dot{R}}{c}\right) R \ddot{R} + \frac{3}{2} \dot{R}^2 \left(1 - \frac{\dot{R}}{3c}\right) = \left(1 - \frac{\dot{R}}{c}\right) \frac{P}{\rho_L} + \frac{R}{\rho_L c} \dot{P} \quad (5)$$

where P is given by

$$\begin{aligned} P &= \left(p_{stat} - p_v(T_\infty) + \frac{2S}{R_0}\right) \left(\frac{R_0}{R}\right)^{3k} - \frac{2S}{R} - \frac{4\mu_L \dot{R}}{R} - p_{stat} \\ &\quad + p_v(T_\infty) - A \sin(2\pi f t) \end{aligned} \quad (6)$$

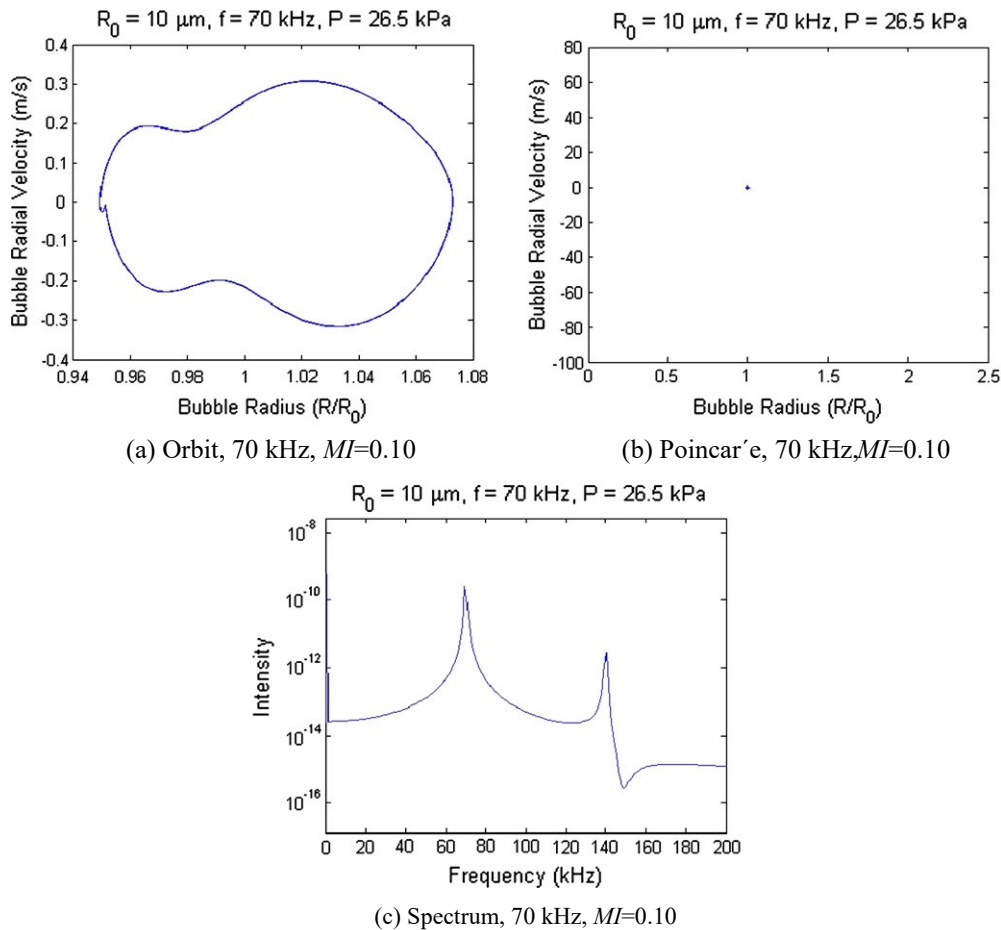


Fig. 2. For a single 10- μm bubble at 70 kHz applied pressure and at a $MI = 0.10$: (a) trajectory in state space projection, (b) Poincaré section plot, and (c) frequency spectrum.

Mach number. Their versions, however, require the driving pressure expression shown above to contain a retarding term in its argument, that is

$$p_\infty(t) = p_{stat} + A \sin(2\pi f(t + R/c))$$

where c is the speed of sound in water which complicates the definition of the subsequent Poincaré map. Parlitz et al. [35] ignore this term in their analysis and show that their modification and the

We can now introduce the variables $u = \dot{R}$ and $\Theta = f t \text{ mod } 1$, just as before to transform the Keller–Miksis–Parlitz equation into a system of three autonomous differential equations:

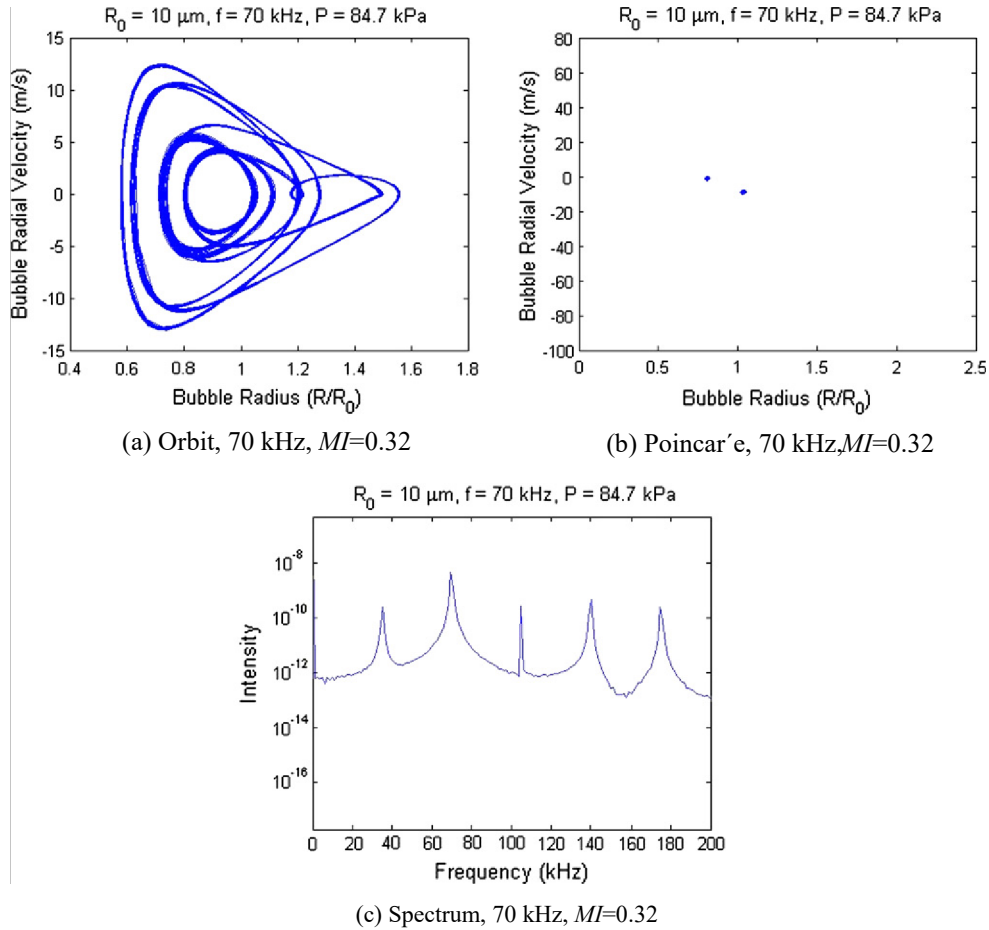


Fig. 3. For a single 10- μm bubble at 70 kHz applied pressure and at a $MI = 0.32$: (a) trajectory in state space projection, (b) Poincaré section plot, and (c) frequency spectrum.

$$\begin{aligned}
 \dot{R} &= u \\
 \dot{u} &= \left[\left(1 - \frac{u}{c}\right)R + \frac{4\mu_L}{\rho_L c} \right]^{-1} \left[-\frac{u^2}{2} \left(3 - \frac{u}{c}\right) \right. \\
 &\quad + \left(1 + (1 - 3k)\frac{u}{c}\right) \left(\frac{p_{star} - p_v(T_\infty)}{\rho_L} + \frac{2S}{\rho_L R_0} \right) \left(\frac{R_0}{R} \right)^{3k} \\
 &\quad - \frac{2S}{\rho_L R} - \frac{4\mu_L}{\rho_L} \frac{u}{R} - \left(1 + \frac{u}{c}\right) \frac{p_{star} - p_v(T_\infty) + A \sin(2\pi\Theta)}{\rho_L} \\
 &\quad \left. - R \frac{2\pi f}{\rho_L c} A \cos(2\pi\Theta) \right] \\
 \dot{\Theta} &= f
 \end{aligned} \tag{7}$$

The dynamics of this system were calculated using a Runge–Kutta routine in a standard MATLAB adaptive solver (ode45).

Difficulties in the integration of the system above arise when the oscillations in bubble radius contain the sharp downward peaks that are characteristic of bubble collapse. Either more sophisticated algorithms or a smaller time step can resolve this difficulty, adding to the computation time [35]. Parlitz et al. circumvented this problem by integrating a topologically equivalent system that smoothed out the singularities. Their approach was used in this research whenever the integration procedure was unable to handle the singularities arising in the Keller–Miksis–Parlitz model and it inevitably “blew up.” Briefly, the original system is transformed

into a new one that allowed for smoother oscillations but also retained all of its qualitative, topological properties. This is accomplished by means of the following diffeomorphism from the state space [35] into its topologically equivalent space:

$$\begin{aligned}
 x_1 &= \alpha \exp\left(\frac{\beta R}{R_0}\right) \\
 x_2 &= \gamma u \exp\left(\frac{\beta R}{R_0}\right) \\
 x_3 &= \Theta
 \end{aligned} \tag{8}$$

where the parameters α , β and γ control the smoothness of the oscillations in the new space. Time is also rescaled: $t' = f_0 t$, where $f_0 = \alpha\beta/\gamma R_0$, and differentiation is with respect to rescaled time.

A MATLAB program was written to solve this system whenever the inward oscillations leading to collapse calculated from Equation 7 became so pronounced that the standard solver (ode45) was unable to yield reasonable values. The details are found elsewhere [47]. The values used for the control parameters in the transformation were: $\alpha = 1$, $\beta = 2$, and $\gamma = 0.001$, as reported by Parlitz et al. [35].

The initial conditions used in the dynamic calculations were $R_0 = 10 \mu\text{m}$, $u = 0 \text{ m/s}$, and $\Theta = 0$. The driving frequency was set at 70 kHz, the parameters in Table 1 were those for water at 25 C, and the oscillations were assumed adiabatic with $k = 1.4$ [35]. Trajectories were plotted once transients disappeared, which normally occurred

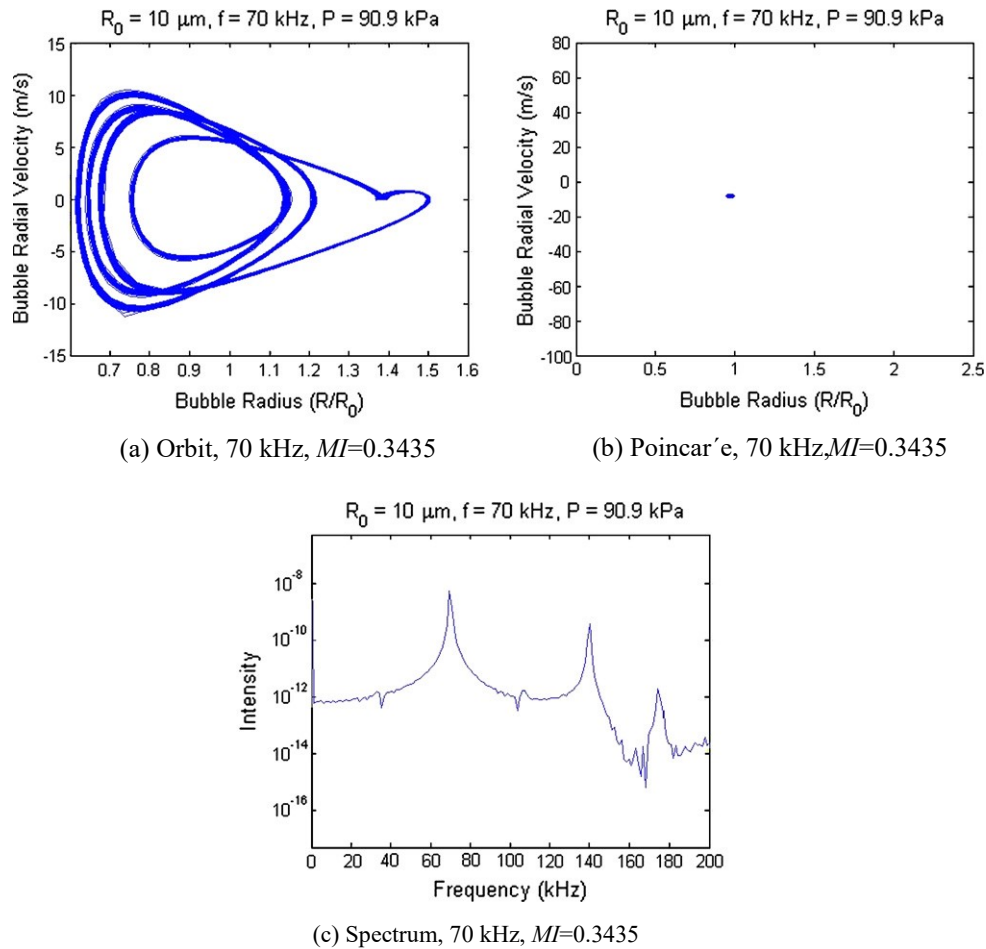


Fig. 4. For a single 10- μm bubble at 70 kHz applied pressure and at a $MI = 0.3435$: (a) trajectory in state space projection, (b) Poincaré section plot, and (c) frequency spectrum.

after about 250 ls. The calculations were done as a function of the mechanical index (MI) parameter. The MI is often used by experimentalists and radiologists to estimate the probability of inertial cavitation events, and is given by $MI = (P/\text{MPa}) / (f/\text{MHz})^{1/2}$ [48,49], where P is the peak negative pressure, and is equivalent to A (for a sinusoidal wave) in Table 1.

It is important to note that these models are, of course, an overly simplified reflection of the experimental conditions. First and foremost, the models trace the behavior of only a single bubble under an external applied pressure, ignoring the coupling effects found in bubble clusters [29–31] and the possibility that some Pluronic polymer may have accumulated at the gas–liquid interface. We found this acceptable since we seek only a qualitative sketch of how a bubble behaves at the parameters at which the experiments were run. Second, the initial bubble size is kept constant for all frequencies and pressures used in these calculations. The objective was to observe the qualitative bubble behavior at 70 kHz; the 10- μm bubble size is typical of naturally occurring air bubbles in water [34,35]. In effect, by doing so, we are looking at a slice of parameter space, a space which is vast and highly complex [24]. Additionally, by considering a single bubble of a given initial size, it is easier to study an acoustic signal in particular. This helps to separate behavior directly related to drug subharmonic) from acoustic signals that may not be directly related

baseline shift). This is exemplified in the acoustic spectra shown in Fig. 1, where only the subharmonic correlates with drug release [9,10] and the background noise shift is more likely a result of collapsing bubbles of a different resonant size. Furthermore, even though the micellar drug carrier was present as a surfactant in the experiments, its effect on bubble size distribution was not considered for this initial study.

We realize that gas bubbles in the presence of micelles will collect some of the Pluronic block copolymer at the gas liquid interface. However, the literature contains no reports of experiments or models regarding the phenomenon for block copolymers at the interface of oscillating gas bubbles. As a first approximation, we expect that the surface energy would be lower and the fluid viscosity at the interface greater, but it is difficult to predict the extent. Therefore, this model of oscillations did not include these complications. The dynamics of bubble oscillations can change with the presence of a surfactant, and more research is needed to further explore this point. The implications are that the actual bubbles are probably damped in their oscillation by the polymers at their interface; this will probably require a higher acoustic pressure than predicted in models without polymers at the interface, which is in the correct direction of the experimental observation in that the experimental MI for subharmonic bubble behavior is higher than the

to it
(such
as

MI calculated from the bubble dynamic model. However, since this is pure speculation without support, we will not discuss it further in this paper.

Finally, we must remember that the experimental signal generated by the 70-kHz source is actually a 70-kHz (continuous) wave amplitude modulated sinusoidally at about 0.12 kHz. This might explain the noisy appearance of the 70 kHz spectra (Fig. 1) compared to other experimental spectra generated at 500 kHz [47]. The clean driving pressure model used for the calculations at 70 kHz is thus an approximation deemed appropriate since we are interested solely in exploring the dynamics arising at this frequency. It is also important to note here that the noisiness observed in the hydrophone was similar to the noisiness observed when measuring the voltage output from the

investigating the resulting phase portraits two-dimensionally. The result is a limit cycle (an isolated closed trajectory) that appears (incorrectly) to cross itself, a consequence of the elimination of the extra dimension.

We employ the Poincaré map from Strogatz [50]. Poincaré maps are a convenient visual tool to identify the periodicity of each point in the domain. These maps make it trivial to identify the signature, and to identify whether the system exhibits a smear or a fractal behavior/representation. The measurement of spectra and the Poincaré maps complement each other, the latter allowing one to move from the realm of continuous dynamical systems to the more intuitive world of discrete maps. Unfortunately, it is rarely possible to find an explicit form of the map and here we rely on the

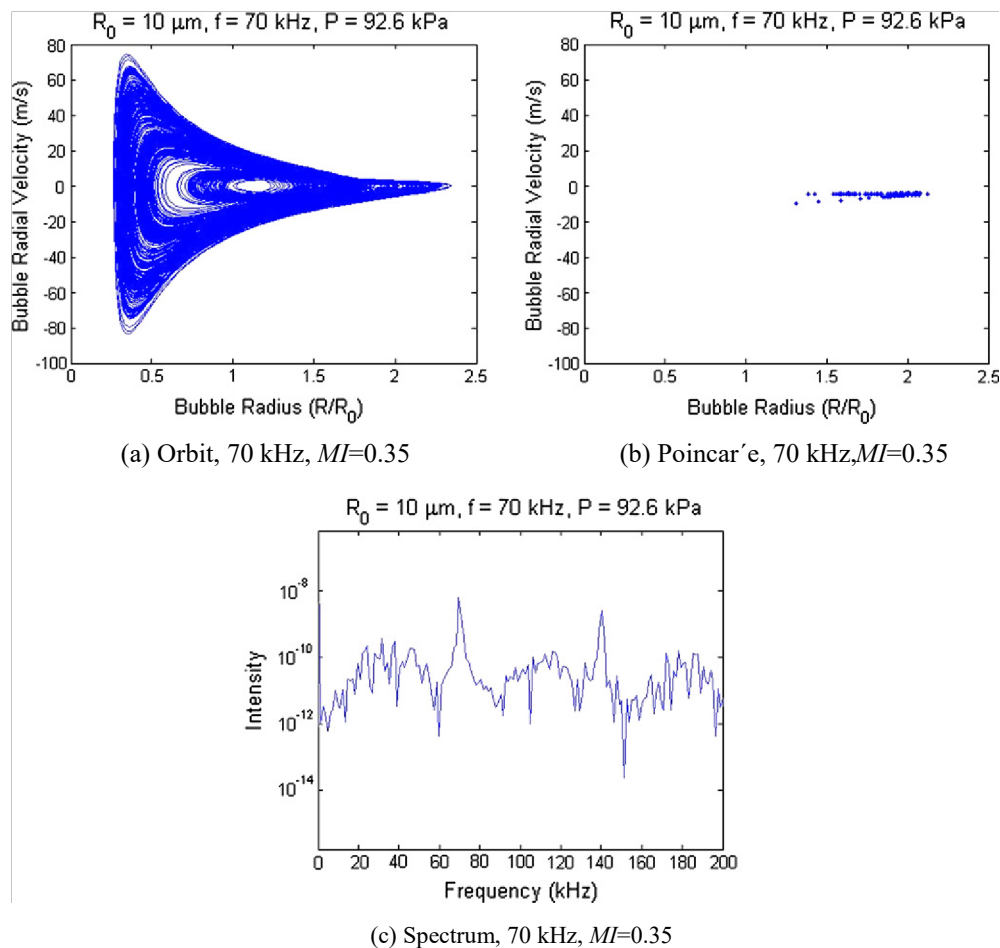


Fig. 5. For a single 10- μm bubble at 70 kHz applied pressure and at a $MI = 0.35$: (a) trajectory in state space projection, (b) Poincaré section plot, and (c) frequency spectrum.

circuit driving the piezoelectric transducer. Therefore, it may be safe to conclude that the noisiness is coming from the circuit and is independent of the bath geometry.

The state space given by the equations described above is three-dimensional, so trajectories of any given initial conditions should trace a three-dimensional shape. The definition of the variable H leads to a convenient state space: the conic section traced by the smooth oscillations gives a torus-like state space [35]. Hence, the evolution of the variable H reflects the number of revolutions of a particular trajectory around this state space. One can then generate a projection of both R and u , eliminating H and

numerical approximations of the ODE solver. Note that if x is a fixed point (i.e., $P(x) = x$), then a trajectory starting at x returns to x after some time T and is therefore a closed orbit for the original system. Hence, when plotting the Poincaré map, any attracting limit cycles generated by the bubble equations will result in single points. For example, if the bubble is oscillating at the driving frequency f , a single point should appear. If the bubble, however, begins oscillations at twice the period of the applied pressure (that is to say, at half the frequency, $f/2$), then two points should appear on the plane, and so forth. In nonlinear dynamical systems such as the one analyzed here, it is common to find another type of

attractor, called a strange attractor. This is no longer a point, curve, or surface, but a fractal, and will reveal itself on the Poincaré cross-section as a type of “smearing” of points with self-similar structure [34,35,50].

3. Results

A stable limit cycle is created for low pressures as Fig. 2 reveals, which is a representative case with a pressure of 26.5 kPa ($MI = 0.10$). The orbit shown in Fig. 2a has a slight pinching near $R/R_0 = 1$. The Poincaré cross-section (Fig. 2b) and frequency spectrum (Fig. 2c) show that the bubble is oscillating at the driving frequency and hence a single fixed point appears and the fundamental and second harmonic peaks are visible.

The “pinching” of the orbit reflects velocity variations as the bubble contracts and expands. In particular, the bubble achieves its highest velocities when $R > R_0$, a rather unusual observation. Also, the bubble tends to momentarily slow down whenever it reaches a radius of about 99 % of its equilibrium radius R_0 . We suspect that this behavior is a consequence of the low driving frequency for this size of bubble. A first-order estimate for the resonance frequency of an air bubble in water is [51]

$$f_{\text{res}} = 3.3\text{m/s}/R_0$$

and thus our bubble has a resonance frequency of about 330 kHz, which is greater than the applied frequency. The bubble dynamics at this frequency are under what Leighton [51] calls “stiffness control”, and the bubble, in general after initial transients, expands when pressure decreases. The compressibility of the gas, not the momentum of the fluid, dominates the bubble dynamics.

The solutions continue to show this “pinching” as the pressure amplitude is increased and the bubble oscillates at a frequency less than its resonance. Eventually, the acceleration of the bubble wall at low radii begins to dominate and we see a different orbit wherein the highest velocities are achieved at low radii, as seen in Fig. 3a. The pressure amplitude in Fig. 3 is 84.7 kPa with a $MI = 0.32$. The orbit looks like a complicated series of twists and turns, and the Poincaré cross-section (Fig. 3b) reveals a surprising detail: the period has doubled, showing two clear isolated points. The frequency spectrum (Fig. 3c) confirms this, showing the appearance of the subharmonic ($f/2 = 35$ kHz) signal. The “velocity pinching” mentioned above remains as well. In fact, it seems that, as the pressure increases, the bubble struggles with being out of phase with the incoming wave more and more, leading to a jagged velocity profile.

The period doubles at $MI = 0.32$, the computational subharmonic threshold. Note that the experimental threshold (in MI) was found to occur between 0.35 and 0.40 [9,10]. Considering the limitations of the model presented here, especially the fact that a single bubble is being modeled and not a more realistic cluster of bubbles, the values show remarkable agreement. This suggests that, at least as far as subharmonics go, the bubble–bubble interaction is not the dominant parameter at these conditions.

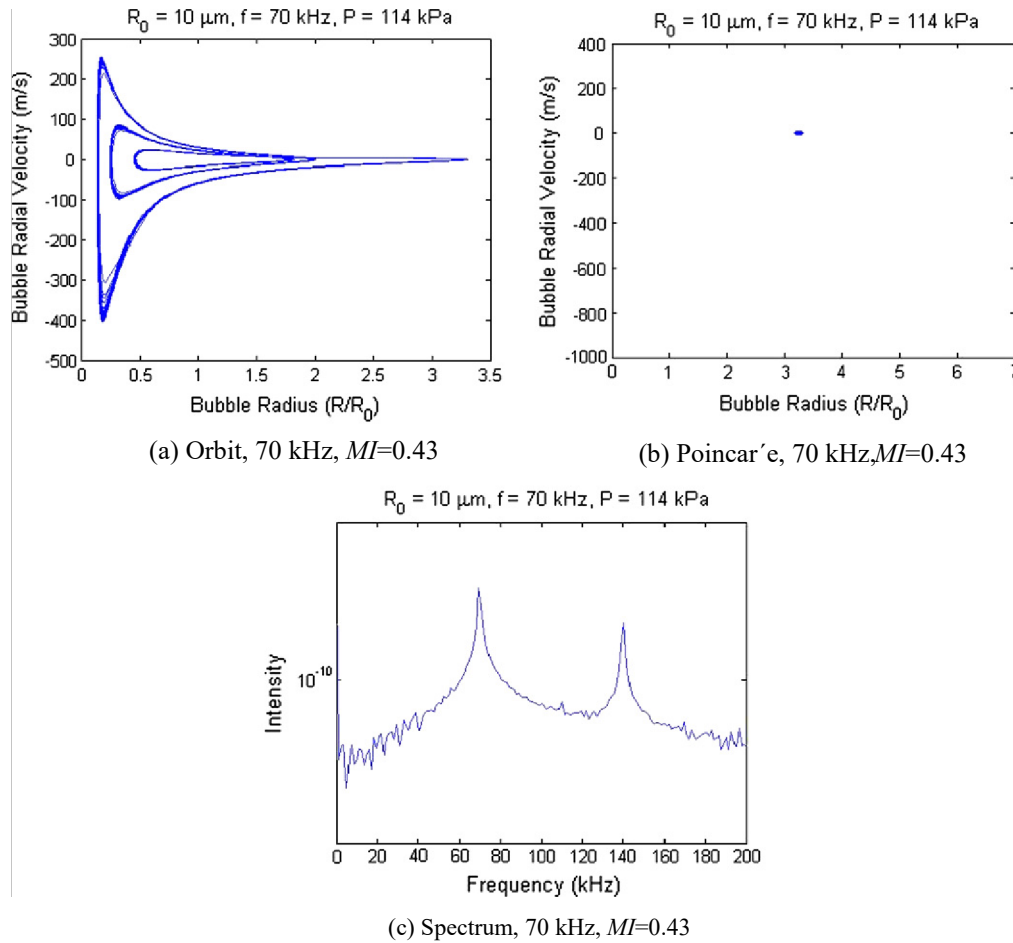


Fig. 6. For a single 10- μm bubble at 70 kHz applied pressure and at a $MI = 0.43$: (a) trajectory in state space projection, (b) Poincaré section plot, and (c) frequency spectrum.

Slightly increasing the driving pressure after the seeming disappearance of the double-period orbit unexpectedly sends the system into chaos. Fig. 5 presents results for a slightly higher pressure of 92.6 kPa ($MI = 0.35$) almost immediately following the stable double-period orbit shown above. The orbit projection (Fig. 5a) reveals the strange attractor that is created. Although the Poincaré cross-section (Fig. 5b) does not yet show a complete fractal shape, the frequency spectrum confirms the chaos created with its noisy, raised baseline (Fig. 5c).

The results shown in Fig. 5 find the bubble eschewing the conventional route to chaos by a series of infinitely many period doublings seen in other systems [52]. Instead, the bubble oscillation develops a double period for a short time before creating all periods almost instantly. This apparently direct and sudden transition from some type of stable oscillation into a strange attractor is generally known as the intermittent route to chaos [53]. It arises out of a kind of bifurcation known as a saddle-node bifurcation of cycles (or fold), which, roughly, is concerned with the birth and/or destruction of stable and unstable limit cycles [50,54]. All it takes to reach chaos is a single saddle-node bifurcation, although it could be the result of a series of them; the presence of this type of route to chaos in bubble oscillators has been reported by Lauterborn and Parlitz [34].

The resulting chaotic oscillations persist before ending as abruptly as they commenced. At approximately 114 kPa

($MI = 0.43$), a stable limit cycle is created out of the strange attractor (Fig. 6a). The Poincaré cross-section (Fig. 6b) accordingly shows a fixed point while the return of the fundamental peak (and its integer harmonics) is seen in the frequency spectrum (Fig. 6c). It is noteworthy not only that the strange attractor disappears and a single-period stable limit cycle is created but that this new oscillation is not necessarily a return to the original fundamental oscillation (for $MI < 0.32$). A comparison of Figs. 3a and 6a shows that the new cycle is not only wider but also much faster, with dramatic accelerations at low radii. The maximum inward velocity in Fig. 5a is revealing in that it has exceeded the speed of sound in air at the simulation conditions, which is approximately 350 m/s. This is most likely evidence of a bubble collapse as the incoming bubble wall is moving faster than the speed of sound in the gas phase, creating a density discontinuity and a shock wave. The model predicts a symmetric collapse and so mathematically the bubble bounces back to continue oscillating. In reality, bubble–bubble interactions will cause the bubble to collapse asymmetrically and fragment into smaller bubbles, whose smaller sizes would place their resonance frequency even further from the applied 70 kHz. Although probably no longer representing

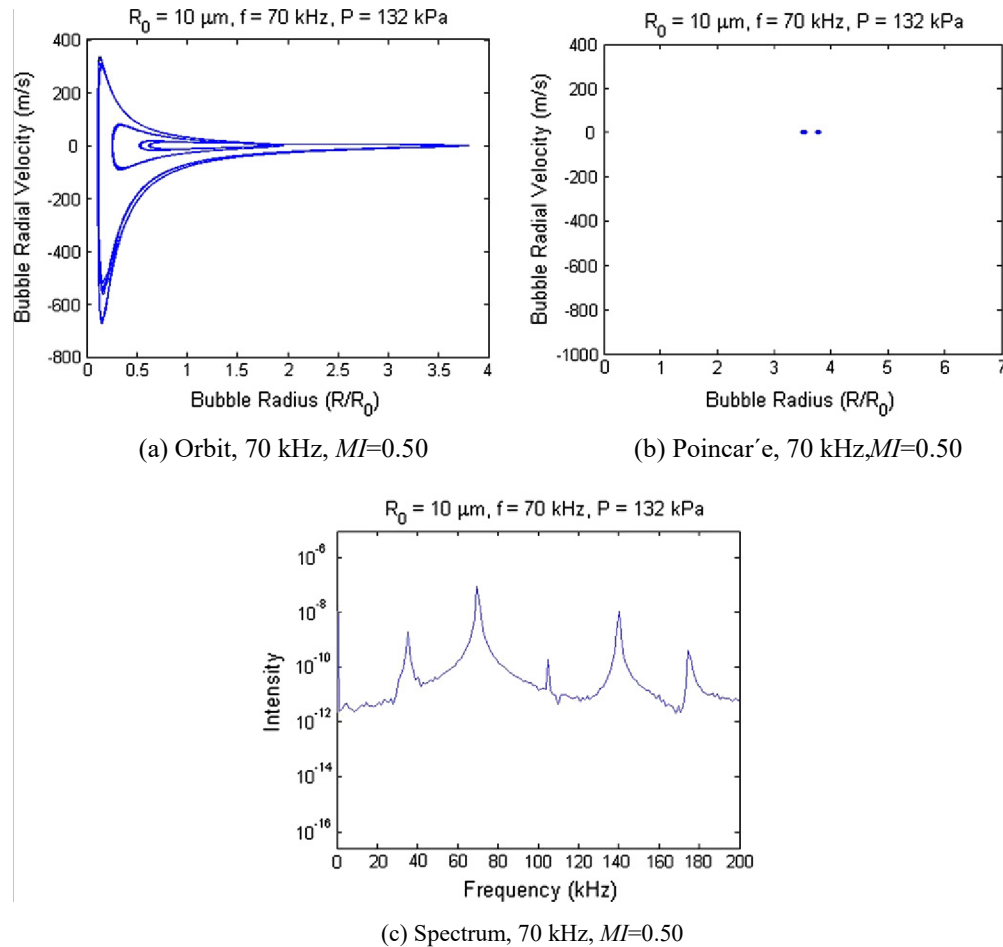


Fig. 7. For a single 10- μm bubble at 70 kHz applied pressure and at a $MI = 0.50$: (a) trajectory in state space projection, (b) Poincaré section plot, and (c) frequency spectrum.

experimental bubble behavior, we will still continue our description of this very interesting bubble dynamic behavior.

As will be shown shortly, for increasing pressures, the bubble wall velocity will continue to exhibit this behavior, and we can say that the bubble is in a collapsing regime. The oscillations, however, do not remain as a stable limit cycle and so we investigate how the new chaotic regime is achieved.

First, at some point just before $A = 132 \text{ kPa}$ ($MI = 0.50$), the system undergoes another period-doubling bifurcation (Fig. 7). A close examination of the resulting limit cycle in Fig. 7a reveals the second loop trailing closely to the original cycle, leading to a second point on the Poincaré plot (Fig. 7b) and the reemergence of the subharmonic peak in the frequency spectrum (Fig. 7c).

The bubble's motions keep increasing in velocity as the bubble collapses, as the projected orbit shows in Fig. 7a. The velocity is close to zero at the equilibrium radius with most of the acceleration concentrated at very low radii ($R/R_0 < 0.1$), close to collapse. Also, the bubble wall achieves its maximum velocity as it contracts close to collapse, at almost twice the velocity attained as when it expands.

The bubble's behavior is starting to look familiar. Instead of creating a single-period oscillation before launching into chaos however, the two points on the Poincaré plot keep moving apart from each other. At a pressure of about 140 kPa ($MI = 0.53$), the first indications of chaos begin to appear (Fig. 8). The strange attractor is not clearly visible yet (the cycle seems to be slowly winding into

itself, see Fig. 8a), and the system appears to be stuck in the transition between stable double-period oscillations and chaos, as seen in the frequency spectrum (Fig. 8c), where the subharmonic remains amidst a raised and noisy baseline. This behavior is common in the intermittent route to chaos, where the system moves between stable oscillations (at the period immediately preceding chaos) and short bursts of chaotic motion (hence, "intermittent"). These "laminar phases" eventually disappear into full chaos [13]. Predictably, the Poincaré cross-section (Fig. 8b) begins to show the stretching of periodic points as they start to form the fractal indicative of chaos.

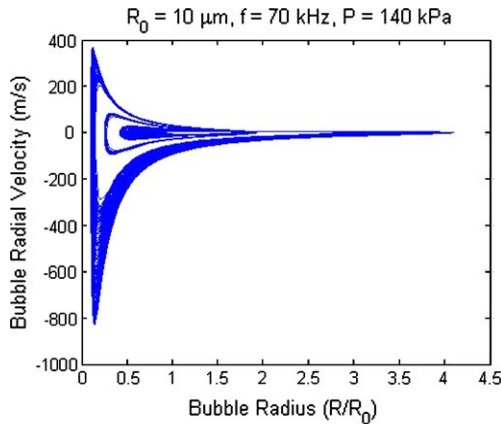
A new strange attractor is formed for values of $A > 140 \text{ kPa}$ ($MI > 0.53$) containing oscillations of all periods. There are several windows within the chaotic regime where oscillations of period three are present, such as at $A = 148 \text{ kPa}$ ($MI = 0.56$) (Fig. 9). The orbit (Fig. 9a) looks self-similar but without a multitude of winding trajectories within it resulting from all periods being present (hinting that they may be temporarily invisible to the computer).

The frequency spectrum (Fig. 9c) reveals sharp peaks at $f/3 = 23.3$ and $2f/3 = 46.6$ with a small shoulder all that remains of the $f/2$ subharmonic signal. This suggests the existence of periodic points of period three in discrete space, confirmed by the Poincaré cross-section in Fig. 9b. Points of period three are important oddities in discrete dynamical systems, as expounded in the famous result of Sarkovskii [52]. In our case, if we restrict our Poincaré map to the real line (by, for example, collapsing it onto the radius or velocity

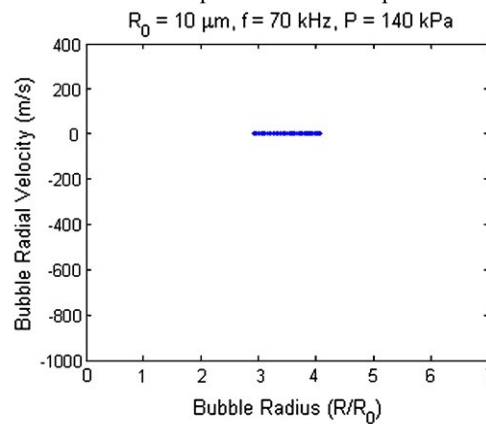
axis) and it is continuous, then a periodic point of period three implies the existence of points of all other periods, even if a numerical algorithm remains blind to them. Consider the following

Thus, the existence of periodic points of period three implies the existence of periodic points of all periods, even if a numerical algorithm remains blind to them.

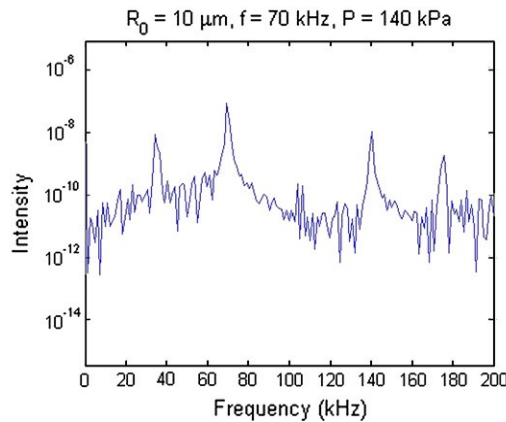
This chaotic pattern continues up to and beyond $MI = 0.70$, with a



(a) Orbit, 70 kHz, $MI=0.53$



(b) Poincaré, 70 kHz, $MI=0.53$



(c) Spectrum, 70 kHz, $MI=0.53$

Fig. 8. For a single 10- μm bubble at 70 kHz applied pressure and at a $MI = 0.53$: (a) trajectory in state space projection, (b) Poincaré section plot, and (c) frequency spectrum.

ordering of N (known as Sarkovskii's ordering of the natural numbers):

$$3 \triangleright 5 \triangleright 7 \triangleright \dots \triangleright 2 \cdot 3 \triangleright 2 \cdot 5 \triangleright \dots \triangleright 2^2 \cdot 3 \triangleright 2^2 \cdot 5 \triangleright \dots \triangleright 2^3 \cdot 3 \triangleright 2^3 \cdot 5 \triangleright \dots \triangleright 2^3 \triangleright 2^2 \triangleright 2 \triangleright 1,$$

where all odd numbers (except 1) are listed first, followed by 2 times the odds, 2^2 times the odds, and so forth, leaving the powers of 2 for last, followed by 1. The theorem is:

Sarkovskii's Theorem: Let $f : \mathbb{R} \rightarrow \mathbb{R}$ be continuous. Suppose f has a periodic point of prime period k . If $k \cdot 1$ in the above ordering, then f also has a periodic point of period 1.

The theorem above is taken from Devaney [52], who also provides a basic proof. This theorem is remarkable for its simple hypothesis and strong result. The obvious corollary that concerns us is:

Corollary. Let $f : \mathbb{R} \rightarrow \mathbb{R}$ be continuous. Suppose f has a periodic point of period three. Then f has periodic points of all other periods.

strange attractor creating oscillations of all periods along with windows of periodic points of period three. An example of the chaos encountered at these values is given Fig. 10, where $A = 153$ kPa and $MI = 0.58$.

As expected, the projected orbit (Fig. 10a) retains the basic shape seen before with the addition of self-similar windings and twists within it. The Poincaré plot (Fig. 10b) tells little, perhaps due to the time interval of integration not allowing for a full picture to form. The frequency spectrum confirms the chaotic nature of the system at this pressure value; Fig. 10c shows an increase in background noise, indicative of the presence of all frequencies.

4. Discussion

The results of the experimental observations of drug release at 70 kHz show that there is a threshold at about $MI = 0.37$ for the onset of drug release from the micellar drug carriers as shown in Fig 11. At higher values of MI , the amount of drug released increases, and then levels off, which is considered to indicate a steady state balance of released and re-encapsulated drug [9,10].

The MI is used as a parameter in this paper because it is a value that can be interpreted in terms of the probability or intensity of inertial cavitation occurring. As a definition and equation ($MI = P/\sqrt{f}$) calculated for any frequency and acoustic pressure. However, the numerical data of Apfel and Holland [48] from which the MI is derived show that the MI as defined slightly underestimates the cavitation threshold at frequencies below 750 kHz. Thus at 70 kHz, the onset of chaotic cavitation in water may occur at higher acoustic pressures (and higher values of MI) than one would expect from the general correlation of thresholds at frequencies above 1 MHz. We find it remarkable that the experimental observation of drug

release occurs at slightly higher acoustic pressures than one would expect from modeling the onset of chaotic behavior in this simplified system at 70 kHz.

A closer examination of the subharmonic component of the experimental frequency spectrum (see Fig. 12) shows not only a threshold, but a log-linear relationship between the subharmonic (35 kHz) intensity and the amount of drug released. The threshold in MI corresponds to a subharmonic threshold of about 0.002 IW/cm^2 . Interestingly, there are three data points that lie to the right (higher values of MI) of the correlation line, and appear to be repeatable. These indicate the presence of a large subharmonic intensity ($>0.35 \text{ IW/cm}^2$), but very little drug release ($<1\%$). We will come back to this observation later.

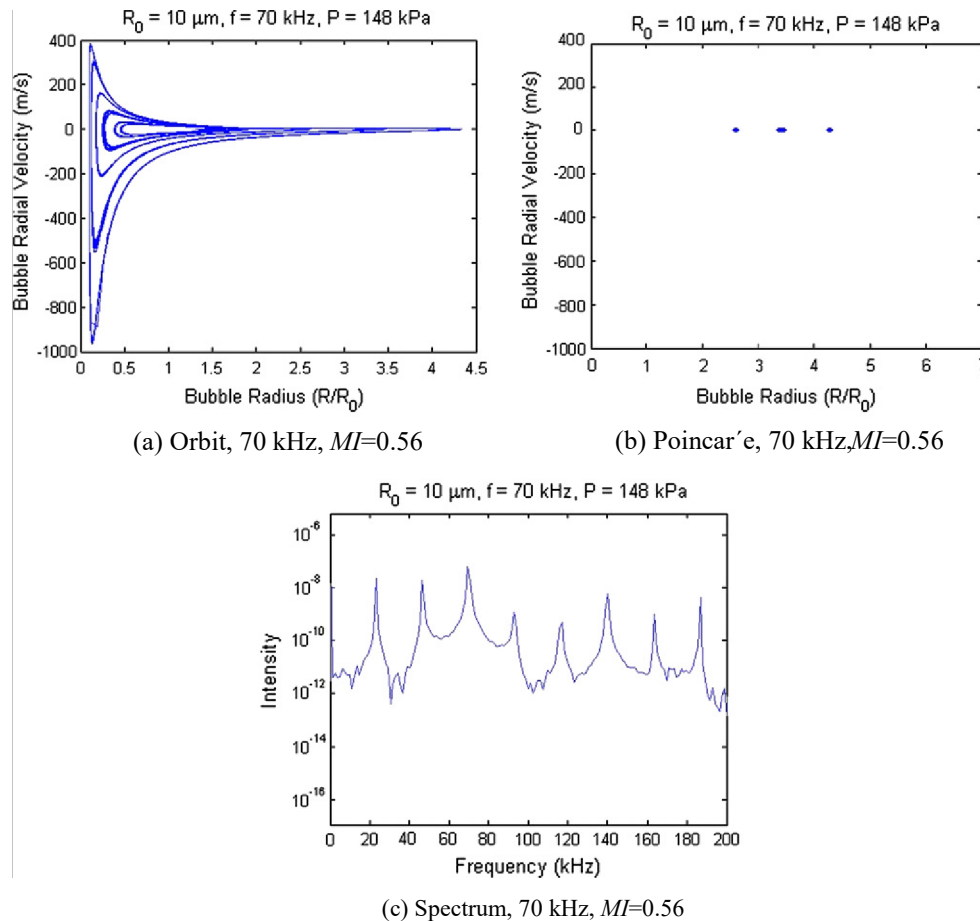


Fig. 9. For a single 10- μm bubble at 70 kHz applied pressure and at a $MI = 0.56$: (a) trajectory in state space projection, (b) Poincaré section plot, and (c) frequency spectrum.

release occurs at slightly higher acoustic pressures than one would expect from modeling the onset of chaotic behavior in this simplified system at 70 kHz.

A closer examination of the subharmonic component of the experimental frequency spectrum (see Fig. 12) shows not only a threshold, but a log-linear relationship between the subharmonic (35 kHz) intensity and the amount of drug released. The threshold in MI corresponds to a subharmonic threshold of about 0.002 IW/cm^2 . Interestingly, there are three data points that lie to the right (higher values of MI) of the correlation line, and appear to be repeatable. These indicate the presence of a large subharmonic intensity ($>0.35 \text{ IW/cm}^2$), but very little drug release ($<1\%$). We will come back to this observation later.

release threshold (between 0.35 and 0.40 in mechanical index) suggested that cavitation was responsible for drug release. Acoustic spectra confirmed this suspicion as subharmonic intensity correlates faithfully with drug release, the signal appearing at the same time as the onset of release. Bubble collapse occurred before drug release was detected, implying that the subharmonic oscillations involved in drug release are independent of the violent collapse associated with acoustic signatures such as the increase in background noise. We posit that shear waves caused by cavitation events that produced the $f/2$ subharmonic also aid in shearing micelles open, thus releasing their drug content to the surrounding solution.

We summarize the findings of the dynamic simulation in what is called a bifurcation diagram. In the realm of discrete dynamical

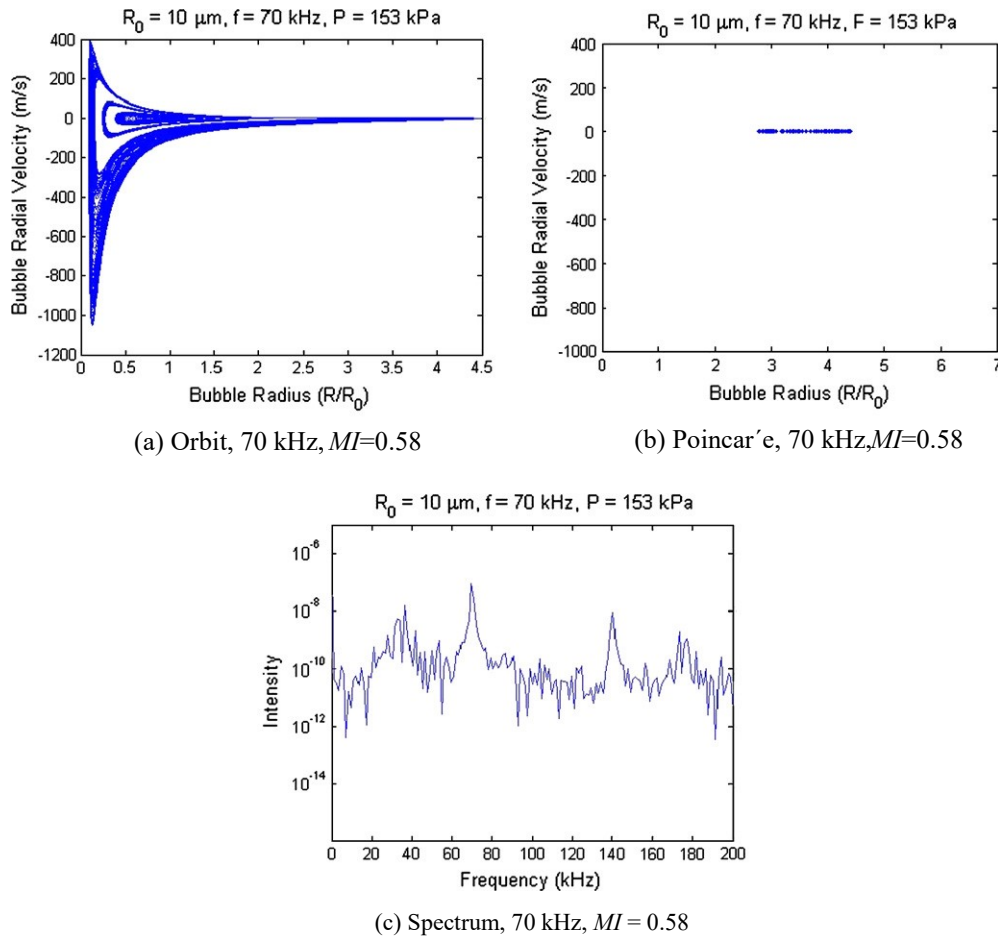
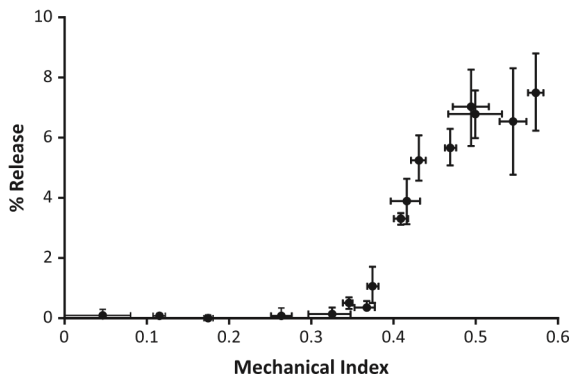


Fig. 10. For a single 10- μm bubble at 70 kHz applied pressure and at a $MI = 0.58$: (a) trajectory in state space projection, (b) Poincaré section plot, and (c) frequency spectrum.



systems, a bifurcation diagram simply plots the periodic points (including fixed points) of a map against a control parameter. Thus, they contain the entire dynamic history of the system for the parameter of interest. For the system of differential equations studied in this research, the link between the continuous and discrete is the Poincaré plot. Even if we cannot find its explicit analytic form, the qualitative results presented above allow us to create a rough sketch of the bifurcation diagram. We choose the bubble radius given by the Poincaré map (after Parlitz et al. [35]) as the state variable for the bifurcation diagram.

Fig. 13 presents the bifurcation diagram as a function of the mechanical index (MI) for 70 kHz. This plot effectively summarizes the results previously presented in this paper and shows what is

termed an intermittent route to chaos. Not only does classical period-doubling never happen beyond points of period two, but the chaotic regime intervals are fairly narrow and seem to follow an increasing R/R_0 pattern.

The seemingly discontinuous jumps in R/R_0 as the MI increases are unexpected and appear at the beginning and end of the first chaotic regime ($MI \approx 0.35$ and 0.43). There are at least two possible explanations for this phenomenon. Either it is a result of the dy- Fig. 11. Experimental data showing average percent release of doxorubicin from Pluronic micelles, as a function of MI at 70 kHz. Error bars represent standard deviations ($n > 4$) from the mean.

dynamic structure of the oscillator or it is a numerical artifact arising from the integration algorithm used by MATLAB. Even if the latter is true, the qualitative bubble behavior may still yield valuable insight into bubble dynamics and their impact on drug release.

If the discontinuities are a characteristic of the system structure, they may arise out of saddle-node bifurcations. As explained before, saddle-node bifurcations govern the creation and destruction of limit cycles (through stability of orbits). Discontinuous jumps in bifurcation diagrams are precisely the destruction of a stable limit cycle and the creation of a new stable one (in this case,

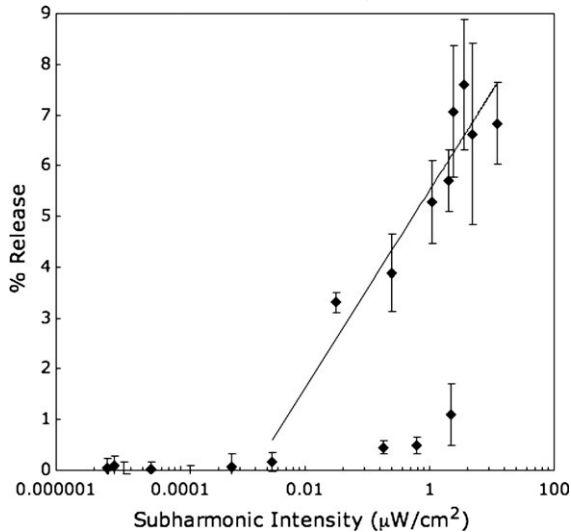


Fig. 12. Percent doxorubicin release from Pluronic micelles correlated with the acoustic intensity of the subharmonic peak. Error bars represent standard deviations from the mean.

one whose conical trajectory has a larger radius). Lauterborn explains this type of bifurcation to some length [34] and presents bifurcation diagrams with similar (seemingly) discontinuous behavior for the bubble oscillator itself [34,35], using the driving frequency as the control parameter rather than the pressure ampli-

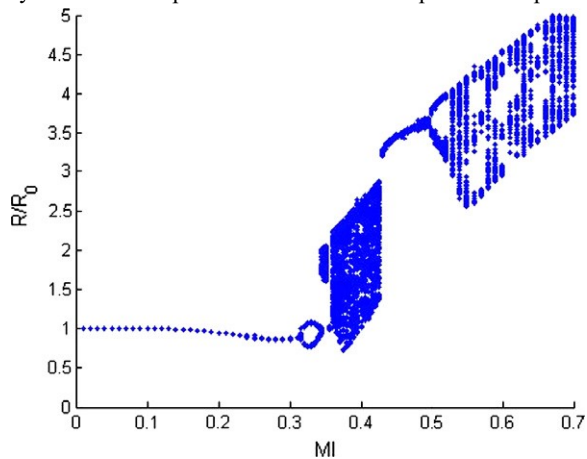


Fig. 13. Bifurcation diagram as a function of mechanical index for a 10 μm bubble at $f = 70$ kHz.

tude as in this work. Lauterborn was the first to report that the acoustic spectrum of cavitating bubbles approached an increased background noise (which he defined as chaos) through successive appearances of half-harmonics of the driving frequency (22.56 kHz). This was the first experiment to physically show the famous period-doubling route to chaos predicted by dynamical systems theory, and which is characteristic of driven nonlinear oscillators. In the previous section we established that the route to chaos at 70 kHz is intermittent, which route proceeds through a single or a series of saddle-node bifurcations. It is therefore reasonable to consider that such a bifurcation created the discontinuities at 70 kHz. The bifurcation diagram in Fig. 13 elegantly illustrates the chaotic nature of the bubble oscillator, in particular, the chaotic map that is created when one moves to discrete space via the Poincaré plot [52].

Given that all periods (i.e., frequencies) are present at the onset of chaos, we can then directly relate the onset of chaos (the appearance of a strange attractor) to the shift in baseline seen in the experiments, which means that background noise does not necessarily imply a collapse event. In fact the low velocities and slight changes in bubble radii shown in Fig. 5 do not suggest that “collapse” is happening. The literature lacks a well-defined criterion to identify a collapse event from the equations of bubble dynamics. The approaches differ by author and include defining the moment of collapse as the point at which the bubble contents reach a temperature of 5000 K [48] and when radial oscillations show “sharp peaks” in the direction of small values ($R/R_0 < 0.1$) of the radius [35]. Using the criterion of bubble wall velocity exceeding the speed of sound in air (explained in the previous section) to identify collapse is sufficient for our qualitative purposes and reveals that the bubble starts collapsing at around a mechanical index of 0.40 at 70 kHz, but not at the lower MI of 0.35 when chaos first appeared. In any case, we can see that collapse is approached by the increasingly violent behavior of the bubble (particularly in its inward movement) as the applied pressure amplitude increases, similar to its approach to chaos.

Ultimately, drug release correlated with the subharmonic signal and not bubble collapse itself (background noise). This is why it is pertinent to focus on the long-term dynamic differences between frequencies and not exclusively on the moment of collapse. It is the subharmonic that still holds the answer. That the subharmonic signal should be intermittent at 70 kHz seems to be confirmed by the three experimental outliers seen in Fig. 12 and mentioned earlier [9]. It is possible that the experimental setup used for 70 kHz (a water bath) created (through hysteresis and/or a distribution of bubble sizes) a wider window of intermittent subharmonic/chaotic oscillations than the bifurcation diagram predicts and that these “quasi-stable” oscillations eventually decreased drastically [34], characterized by the leveling off in percent drug release seen in Fig. 11.

Another conjecture to consider is that there may have been standing waves in the bath, and that the hydrophone was hearing subharmonics from other regions of the acoustic field; but in the volume interrogated by the fiber optic probe, the bubble oscillations were not sufficient (not enough subharmonic intensity) to release

much drug. Such intricacies remain to be explored both experimentally and theoretically.

5. Conclusion

To summarize, drug release from micelles appears to correlate with the intensity of the subharmonic emission in these experiments. There is a threshold for commencement of drug release at a subharmonic intensity of 0.002 IW/cm^2 , and a MI of 0.37. This threshold in MI is very near the MI threshold value (MI = 0.3) at which subharmonic oscillations are predicted by mathematical models of bubble dynamics. In particular for a 10-lm bubble at 70 kHz, the dynamic model predicts that bubble oscillations bifurcate between MI values of 0.32 and 0.34 and then sudden chaotic behavior appears at a MI of 0.35. Obviously, more work needs to be done, both in experiments and models. It would be of particular interest to examine the models of dynamic bubble behavior and drug release at other frequencies, particularly a higher frequency above the resonance frequency of the bubble. Such a case may show very different behavior since the bubble oscillations would be in Leighton's "inertial-controlled" regime instead of the "stiffness-controlled" regime [51]. Experimentally we have observed enhanced drug uptake by cells at 0.5 MHz [4], but we have not observed the same type of drug release from micelles that correlated with the subharmonic signal [47]. Apparently bubble dynamics are very different at 0.5 MHz, as will be discussed in a future paper.

Acknowledgment

The authors would like to acknowledge funding from the National Institutes of Health (R01 CA-98138), the Pope Professorship at Brigham Young University, and the Faculty Research Grant at the American University of Sharjah (FRG-AUS09).

References

- [1] G.A. Hussein, G.D. Myrup, W.G. Pitt, D.A. Christensen, N.Y. Rapoport, Factors affecting acoustically-triggered release of drugs from polymeric micelles, *Journal of Controlled Release* 69 (2000) 43–52.
- [2] G.A. Hussein, N.M. Abdel-Jabbar, F.S. Mjalli, W.G. Pitt, Modeling and sensitivity analysis of acoustic release of doxorubicin from unstabilized Pluronic P105 using an artificial neural network model, *Technology in Cancer Research and Treatment* 6 (1) (2007) 49–56.
- [3] D. Stevenson-Abouelnasr, G.A. Hussein, W.G. Pitt, Further investigation of the mechanism of doxorubicin release from P105 micelles using kinetic models, *Colloids and Surfaces B* 55 (2007) 59–66.
- [4] S.B. Stringham, M.A. Viskovska, E.S. Richardson, S. Ohmine, G.A. Hussein, B.K. Murray, W.G. Pitt, Over-pressure suppresses ultrasonic-induced drug uptake, *Ultrasound in Medicine and Biology* 35 (3) (2009) 409–415.
- [5] B.J. Staples, B.L. Roeder, G.A. Hussein, G.B. Schaalje, W.G. Pitt, Role of frequency and mechanical index in ultrasonic enhanced chemotherapy in rats, *Cancer Chemotherapy and Pharmacology* 64 (3) (2009) 593–600.
- [6] G.A. Hussein, W.G. Pitt, D.A. Christensen, D.J. Dickinson, Degradation kinetics of stabilized Pluronic micelles under the action of ultrasound, *Journal of Controlled Release* 138 (2009) 45–48.
- [7] G.A. Hussein, D. Stevenson-Abouelnasr, W.G. Pitt, K.T. Assaleh, L.O. Farahat, J. Fahadi, Kinetics and thermodynamics of acoustic release of doxorubicin from non-stabilized polymeric micelles, *Colloids and Surfaces A* 359 (2010) 18–24.
- [8] B.J. Staples, B.L. Roeder, G.A. Hussein, W.G. Pitt, Distribution of doxorubicin in rats undergoing ultrasonic drug delivery, *Journal of Pharmaceutical Sciences* 99 (7) (2010) 3122–3131.
- [9] G.A. Hussein, M.A.D. de la Rosa, E.S. Richardson, D.A. Christensen, W.G. Pitt, The role of cavitation in acoustically activated drug delivery, *Journal of Controlled Release* 107 (2) (2005) 253–261.
- [10] G.A. Hussein, M.A.D. de la Rosa, T. Gabuji, Y. Zeng, D.A. Christensen, W.G. Pitt, Release of doxorubicin from unstabilized and stabilized micelles under the action of ultrasound, *Journal of Nanoscience and Nanotechnology* 7 (3) (2007) 1028–1033.
- [11] C.R. Hill, Ultrasonic exposure thresholds for changes in cells and tissues, *The Journal of the Acoustical Society of America* 52 (2) (1972) 667–672.
- [12] G.K. Johri, D. Singh, M. Johri, S. Saxena, G. Iernetti, N. Dezhkunov, K. Yoshino, Measurement of the intensity of sonoluminescence, subharmonic generation and sound emission using pulsed ultrasonic technique, *Japanese Journal of Applied Physics Part 1 Regular Papers Short Notes and Review Papers* 41 (8) (2002) 5329–5331.
- [13] T. Leighton, *The Acoustic Bubble*, Academic Press, London, 1997.
- [14] J.S. Allen, D.E. Kruse, P.A. Dayton, K.W. Ferrara, Effect of coupled oscillations on microbubble behavior, *Journal of the Acoustical Society of America* 114 (3) (2003) 1678–1690.
- [15] C.E. Brennen, *Cavitation and Bubble Dynamics*, Oxford University Press, Inc., 200 Madison Avenue, New York, New York 10016, 1995.
- [16] A. Eller, H.G. Flynn, Generation of subharmonics of order one-half by bubbles in a sound field, *Journal of the Acoustical Society of America* 46 (3) (1969) 722–727.
- [17] H.G. Flynn, C.C. Church, Erratum: Transient pulsations of small gas bubbles in water [*J. Acoust. Soc. Am.* 84, 985–998 (1988)], *Journal of the Acoustical Society of America* 84 (5) (1988) 1863–1876.
- [18] J.L. Mestas, P. Lenz, D. Cathignol, Long-lasting stable cavitation, *Journal of the Acoustical Society of America* 113 (3) (2003) 1426–1430.
- [19] A. Phelps, T. Leighton, The subharmonic oscillations and combination-frequency subharmonic emissions from a resonant bubble: their properties and generation mechanisms, *Acustica* 83 (1) (1997) 59–66.
- [20] S. Zhang, M. Wan, H. Zhong, C. Xu, Z. Liao, H. Liu, S. Wang, Dynamic changes of integrated backscatter, attenuation coefficient and bubble activities during high-intensity focused ultrasound (HIFU) treatment, *Ultrasound in Medicine and Biology* 35 (11) (2009) 1828–1844.
- [21] E. Biagi, L. Breschi, E. Vannacci, L. Masotti, Stable and transient subharmonic emissions from isolated contrast agent microbubbles, *Ieee Transactions on Ultrasonics Ferroelectrics and Frequency Control* 54 (3) (2007) 480–497. 140J.

- [22] A.F. Prokop, A. Soltani, R.A. Roy, Cavitation mechanisms in ultrasound accelerated fibrinolysis, *Ultrasound in Medicine and Biology* 33 (6) (2007) 924–933.
- [23] V. Kamath, A. Prosperetti, Numerical integration methods in gas-bubble dynamics, *Journal of the Acoustical Society of America* 85 (4) (1989) 1538–1548.
- [24] A. Prosperetti, Thermal effects and damping mechanisms in the forced radial oscillations of gas bubbles in liquids, *Journal of the Acoustical Society of America* 61 (1) (1977) 17–27.
- [25] A. Prosperetti, A generalization of the Rayleigh–Plesset equation of bubble dynamics, *Physics of Fluids* 25 (3) (1982) 409–410.
- [26] A. Prosperetti, L.A. Crum, K.W. Commander, Nonlinear bubble dynamics, *Journal of the Acoustical Society of America* 83 (2) (1988) 502–514.
- [27] C.C. Church, Prediction of rectified diffusion during nonlinear bubble pulsations at biomedical frequencies, *Journal of the Acoustical Society of America* 83 (6) (1988) 2210–2217.
- [28] C.C. Church, A theoretical study of cavitation generated by an extracorporeal shock wave lithotripter, *Journal of the Acoustical Society of America* 86 (1) (1989) 215–227.
- [29] I. Akhatov, U. Parlitz, W. Lauterborn, Pattern formation in acoustic cavitation, *Journal of the Acoustical Society of America* 96 (6) (1994) 3627–3635.
- [30] Y. Matsumoto, S. Yoshizawa, Behaviour of a bubble cluster in an ultrasound field, *International Journal for Numerical Methods in Fluids* 47 (6–7) (2004) 591–601.
- [31] R. Omta, Oscillations of a cloud of bubbles of small and not so small amplitude, *Journal of the Acoustical Society of America* 82 (3) (1987) 1018–1033.
- [32] V. Kamath, A. Prosperetti, F. Egolfopoulos, A theoretical study of sonoluminescence, *Journal of the Acoustical Society of America* 94 (1) (1993) 248–260.
- [33] B.-R. Kim, J.-S. Jeon, H.-Y. Kwak, Stability and selective bifurcation for a gas bubble oscillating under ultrasound, *Journal of the Physical Society of Japan* 68 (4) (1999) 1197–1204.
- [34] W. Lauterborn, U. Parlitz, Methods of chaos physics and their applications to acoustics, *Journal of the Acoustical Society of America* 84 (6) (1988) 1975–1993.
- [35] U. Parlitz, V. Englisch, C. Schczyk, W. Lauterborn, Bifurcation structure of bubble oscillators, *Journal of the Acoustical Society of America* 88 (2) (1990) 1061–1077.
- [36] W. Lauterborn, Numerical investigation of nonlinear oscillations of gas bubbles in liquids, *Journal of the Acoustical Society of America* 59 (2) (1976) 283–293.
- [37] W. Lauterborn, E. Cramer, Subharmonic route to chaos observed in acoustics, *Physical Review Letters* 47 (20) (1981) 1445–1448.
- [38] W. Lauterborn, A. Koch, Holographic observation of period doubled and chaotic bubble oscillations in acoustic cavitation, *Physical Review A* 35 (4) (1987) 1974–1976.
- [39] W. Lauterborn, C.-D. Ohl, The peculiar dynamics of cavitation bubbles, *Applied Scientific Research* 58 (1–4) (1998) 53–76.
- [40] A. Prosperetti, Nonlinear oscillations of gas bubbles in liquids: transient solutions and the connection between subharmonic signal and cavitation, *Journal of the Acoustical Society of America* 57 (4) (1975) 810–821.
- [41] W. Lauterborn, E. Suchla, Bifurcation superstructure in a model of acoustic turbulence, *Physical Review Letters* 53 (24) (1984) 2304–2307.
- [42] A. Prosperetti, Subharmonics and ultraharmonics in the forced oscillations of weakly nonlinear systems, *American Journal of Physics* 44 (6) (1976) 548–554.
- [43] A. Prosperetti, Application of the subharmonic threshold to the measurement of the damping of oscillating gas bubbles, *Journal of the Acoustical Society of America* 61 (1) (1977) 11–16.
- [44] L. Samek, A multiscale analysis of nonlinear oscillations of gas bubbles in liquids, *Journal of the Acoustical Society of America* 81 (3) (1987) 632–637.
- [45] J.B. Keller, I.I. Kolodner, Damping of underwater explosion bubble oscillations, *Journal of Applied Physics* 27 (10) (1956) 1152–1161.
- [46] J.B. Keller, M. Miksis, Bubble oscillations of large amplitude, *Journal of the Acoustical Society of America* 68 (2) (1980) 628–633.
- [47] M.A.D. de la Rosa, High-Frequency Ultrasound Drug Delivery and Cavitation, M.S. Thesis, Department of Chemical Engineering, Brigham Young University, Provo, Utah. <<http://contentdm.lib.byu.edu/cdm/singleitem/id/910/collection/ETD>>.
- [48] R.E. Apfel, C.K. Holland, Gauging the likelihood of cavitation from short-pulse, low-duty cycle diagnostic ultrasound, *Ultrasound in Medicine and Biology* 17 (2) (1991) 179–185.
- [49] C.C. Church, Frequency, pulse length, and the mechanical index, *Acoustics Research Letters Online-Arlo* 6 (3) (2005) 162–168.
- [50] S.H. Strogatz, *Nonlinear Dynamics and Chaos*, Westview Press, 1994.
- [51] T.G. Leighton, What is ultrasound?, *Progress in Biophysics and Molecular Biology* 93 (1–3) (2007) 3–83.
- [52] R.L. Devaney, *An Introduction to Chaotic Dynamical Systems, Studies In Nonlinearity*, second ed., Westview Press, Boulder, Colorado, 2003.
- [53] Y. Pomeau, P. Manneville, Intermittent transition to turbulence in dissipative dynamical systems, *Communications in Mathematical Physics* 74 (2) (1980) 189–197.
- [54] M.W. Hirsch, S. Smale, R.L. Devaney, *Differential equations, dynamical systems, and an introduction to chaos*, vol. 60, second ed. *Pure and Applied Mathematics*, Elsevier, San Diego, California, 2004.